

# H<sub>2</sub> in low-ionization structures of planetary nebulae <sup>\*</sup>

Stavros Akras<sup>1</sup> †, Denise R. Gonçalves<sup>1</sup> ‡, Gerardo Ramos-Larios<sup>2</sup>

<sup>1</sup> *Observatório do Valongo, Universidade Federal do Rio de Janeiro, Ladeira Pedro Antonio 43, 20080-090, Rio de Janeiro, Brazil*

<sup>2</sup> *Instituto de Astronomía y Meteorología, Av. Vallarta No. 2602. Col. Arcos Vallarta, CP 44130, Guadalajara, Jalisco, Mexico*

Received **\*\*insert\*\***; Accepted **\*\*insert\*\***

## ABSTRACT

We report the detection of near-IR H<sub>2</sub> emission from the low-ionization structures (knots) in two planetary nebulae. The deepest ever high-angular resolution H<sub>2</sub> 1-0 S(1) at 2.122 μm, H<sub>2</sub> 2-1 S(1) at 2.248 μm and Brγ images of K 4-47 and NGC 7662, obtained using the Near InfraRed Imager and Spectrometer (NIRI) at Gemini-North, are analyzed here. K 4-47 reveals a remarkable highly collimated bipolar structure not only in the optical but also in the molecular hydrogen emission. The H<sub>2</sub> emission emanates from the walls of the bipolar outflows and also from the pair of knots at the tip of the outflows. The H<sub>2</sub> 1-0 S(1)/2-1 S(1) line ratio ranges from ~7 to ~10 suggesting the presence of shock interactions. Our findings can be explained by the interaction of a jet/bullet ejected from the central star with the surrounding asymptotic giant branch material. The strongest H<sub>2</sub> line, v=1-0 S(1), is also detected in several low-ionization knots located at the periphery of the elliptical planetary nebula NGC 7662, but only four of these knots are detected in the H<sub>2</sub> v=2-1 S(1) line. These four knots exhibit an H<sub>2</sub> line ratio between 2 and 3.5, which suggests that the emission is caused by the UV ionizing flux of the central star. Our data confirms the presence of H<sub>2</sub> gas in both fast- and slow-moving low-ionization knots, which has only been confirmed before in the nearby Helix nebula and Hu 1-2. Overall, the low-ionization structures of planetary nebulae are found to share similar traits to photodissociation regions.

**Key words:** ISM: molecules – Interstellar Medium (ISM), Nebulae – infrared: general – planetary nebulae: individual: K 4-47 – planetary nebulae: individual: NGC 7662

## 1 INTRODUCTION

Optical imaging surveys of planetary nebulae (PNe) have revealed that a significant fraction of PNe possess, in addition to large-scale structures such as rims, shells and haloes, various small-scale structures (e.g. Balick 1987; Balick et al. 1998; Corradi et al. 1996; Gonçalves et al. 2001). In these small-scale structures low-ionization emission lines such as [O I], [N II], [O II] and [S II] (low-ionization emission line structures, hereafter LISs) are more prominent than the large scale structures. Moreover, they have a variety of shapes and forms such as knots, jets and filaments (e.g. Gonçalves et al. 2001, and references therein) and cover a wide range of expansion velocities from a few ten of km s<sup>-1</sup>

up to a few hundreds of km s<sup>-1</sup>, indicating a variety of formation and excitation mechanisms.

Shock interactions play a crucial role in the excitation of LISs and provide a plausible explanation for the enhancement of the low-ionization emission lines like [N II], given that there are no chemical abundances variations (e.g. N and O) between the LISs and the surrounding medium (e.g. Gonçalves et al. 2006; Akras & Gonçalves 2016). By studying a sample of five Galactic PNe with LISs and comparing them with theoretical predictions, Akras & Gonçalves (2016) demonstrated that the excitation mechanism of LISs is via a combination shocks and UV-photons emitted from the central star. The contribution of each mechanism depends on a number of physical parameters such as the distance of LISs to the central star, the stellar parameters (T<sub>eff</sub>, L<sub>⊙</sub>), the expansion velocity and the density. The same concept of a mixture of UV-photons produced by shocks and UV-photons emitted from the central star, is also used to explain the bright low-ionization lines in highly evolved PNe (Akras et al. 2016).

The physical properties of LISs such as electron temperature (T<sub>e</sub>), electron density (n<sub>e</sub>) and chemical abundances

<sup>\*</sup> Based on observations obtained at the Gemini Observatory, which is operated by the Association of Universities for Research in Astronomy, Inc., under a cooperative agreement with the NSF on behalf of the Gemini partnership.

† e-mail: akras@astro.ufrj.br

‡ e-mail: denise@astro.ufrj.br

are also of great importance for understanding these structures. They were first studied in detail by Balick and collaborators (Balick et al. 1993, 1994, 1998). The interpretation given by these authors of the [N II] emission line enhancement was the likely overabundance of nitrogen compared with the surrounding medium. Later, Gonçalves and collaborators (Gonçalves et al. 2003, 2009) proved that this is not a necessary condition for explaining the enhancement of the LISs. Akras & Gonçalves (2016) recently shown that the enhancement of low-ionization lines in LISs is the result of their different degree of ionization compared with the rest of the nebula.

Also of importance is the difference in  $n_e$  between the LISs and the other nebular components, as the former are usually found to be less dense than the surrounding medium (Gonçalves et al. 2009). This observational result is inconsistent with the formation models of LISs (e.g. shock models, Dopita 1997; stagnation model, Steffen et al. 2001; magneto-hydrodynamic interacting winds model, García-Segura et al. 2005; binary systems, Soker & Livio 1994), which predict that LISs will be denser than the surrounding medium. An explanation for this discrepancy between the theoretical models and observations could be that the models refer to the total density (dust, atomic and molecular) and not only to the  $n_e$ , which corresponds to the ionized fraction of the gas. Therefore, a possible solution may be that LISs are also made of non-ionized gas (molecular, atomic), as proposed by Gonçalves et al. (2009). This hypothesis is confirmed for a cometary knot in the well studied PN Helix, for which the molecular mass is found to be substantially higher than the ionized mass (Huggins et al 2002; Matsuura et al. 2009). More recently, Fang et al. (2015) detected H<sub>2</sub> emission from the knots of Hu 1-2. Moreover, high-angular resolution images of NGC 2346 in the H<sub>2</sub> v=1-0 line revealed that the equatorial H<sub>2</sub> region of the nebula is fragmented into knots and filaments (Manchado et al. 2015).

H<sub>2</sub> emission is commonly detected in PNe (e.g. Latter et al. 1995; Kastner et al. 1996; Guerrero et al. 2000; Arias et al. 2001; Ramos-Larios et al. 2012; Marquez-Lugo et al. 2015) and proto-PNe (Sahai et al. 1998; Hrivnak et al. 2008) mainly via the bright ro-vibrational v=1-0 transition line of H<sub>2</sub> at 2.122  $\mu$ m. The detection rate of H<sub>2</sub> emission has been found to be higher in bipolar PNe than in other morphological types (e.g. round and/or elliptical). This is known as Gately's rule (Kastner et al. 1994). However, there are some round and elliptical PNe in which H<sub>2</sub> emission has been detected (e.g. the round NGC 6781, Phillips et al. 2011; the elliptical NGC 6720, Latter et al. 1995; NGC 7048, Ramos-Larios et al. 2013; see also Marquez-Lugo et al. 2013). These round and elliptical PNe have central stars with effective temperatures ( $T_{\text{eff}}$ ) >100 kK. Therefore, the high detection rate of H<sub>2</sub> in bipolar PNe may be associated with the high  $T_{\text{eff}}$  of their central stars (Phillips 2006; Aleman & Gruenwald 2004, 2011).

A comparison of H<sub>2</sub> with optical emission line images (e.g. [N II] and [O I]) has revealed very similar morphologies (Guerrero et al. 2000; Bohigas 2001), which suggests that the two emissions originate from the same regions. Theoretical works by Aleman and collaborators (Aleman & Gruenwald 2011; Aleman et al. 2011) have shown that the rovibrational emission of H<sub>2</sub> may be important, not only in the photo-dissociation regions (PDRs) but also in the transition zone

**Table 1.** Observations log

Object	Filter	$\lambda_c$ ( $\mu$ m)	$\Delta\lambda$ ( $\mu$ m)	Time (s)	No. of frames
K 4-47	K-cont-1	2.0975	0.0275	90	9
NGC 7662	K-cont-1	2.0975	0.0275	115	9
K 4-47	H <sub>2</sub> v=1-0 S(1)	2.1239	0.0261	90	9
NGC 7662	H <sub>2</sub> v=1-0 S(1)	2.1239	0.0261	115	9
K 4-47	Brackett $\gamma$	2.1686	0.0295	60	3
NGC 7662	Brackett $\gamma$	2.1686	0.0295	75	3
K 4-47	H <sub>2</sub> v=2-1 S(1)	2.2465	0.0301	155	21
NGC 7662	H <sub>2</sub> v=2-1 S(1)	2.2465	0.0301	190	21 <sup>†</sup>
K 4-47	K-cont-2	2.2718	0.0352	155	21
NGC 7662	K-cont-2	2.2718	0.0352	190	21 <sup>†</sup>

<sup>†</sup> For these observations only 14 out of 21 frames could be used for analysis.

between the ionized and the neutral gas in PNe, a zone containing gas of intermediate ionization degree (see Fig. 4 of Aleman & Gruenwald 2011). Moreover, these authors have shown that the distance from the central star, or equivalently the intensity of the UV radiation field, is a crucial parameter regarding the ionization structure of the knots. Inside the ionization front, knots with high optical depths will exhibit strong H<sub>2</sub>, [N II] and [O I] emission lines, whereas those beyond the ionization front will emit only in the H<sub>2</sub> and [O I] lines (Aleman et al. 2011). Overall, the [O I] emission seems to be a better indicator for the presence of H<sub>2</sub> than the [N II] emission. However, in PNe low-ionization knots, which are dense structures, either [N II] or [O I] emission line would imply the presence of H<sub>2</sub> gas. All cometary knots with [N II] emission in the Helix nebula also exhibit H<sub>2</sub> emission (Matsuura et al. 2009). Moreover, it is worth mentioning that an empirical linear relation between the fluxes of the [O I] 6300 Å emission line and the H<sub>2</sub> v=1-0 for Galactic PNe was proposed many years ago by Reay et al. (1988).

In this paper, we present the detection of H<sub>2</sub> emission from fast- and slow-moving low-ionization knots in two Galactic PNe, namely K 4-47 and NGC 7662. The observations and data analysis are described in Section 2. The results of this work are discussed in Section 3, and the conclusion is presented in Section 4.

## 2 OBSERVATIONS

High-angular-resolution, near-IR narrow-band H<sub>2</sub> (namely v=1-0 S(1) at 2.122  $\mu$ m, v=2-1 S(1) at 2.248  $\mu$ m and Br $\gamma$  at 2.168 $\mu$ m) images of two Galactic PNe with LISs, namely K 4-47 and NGC 7662, were obtained using the Near InfraRed Imager and Spectrometer (NIRI) on the 8 m Gemini-North telescope, at Mauna Kea in Hawaii. The observations were carried out in the service observing mode on 2014 August 6<sup>th</sup> and 2014 October 13<sup>th</sup> (Program IDs: GN2014B-Q43 and GN2014B-Q1).

The observations were carried out in the f/6 configuration (pixel scale = 0.117 arcsec and fields of view of 120 arcsec). The narrow-band G0216, G0218 and G0220 filters, centered at 2.1239, 2.1686 and 2.2465 $\mu$ m, respectively, were applied to isolate the H<sub>2</sub> v=1-0, Br $\gamma$  and H<sub>2</sub> v=2-1 lines, respectively. Continuum images adjacent to the above lines were also obtained, using the corresponding filters centered at 2.0975  $\mu$ m (G0217) and 2.2718  $\mu$ m (G0219), which al-

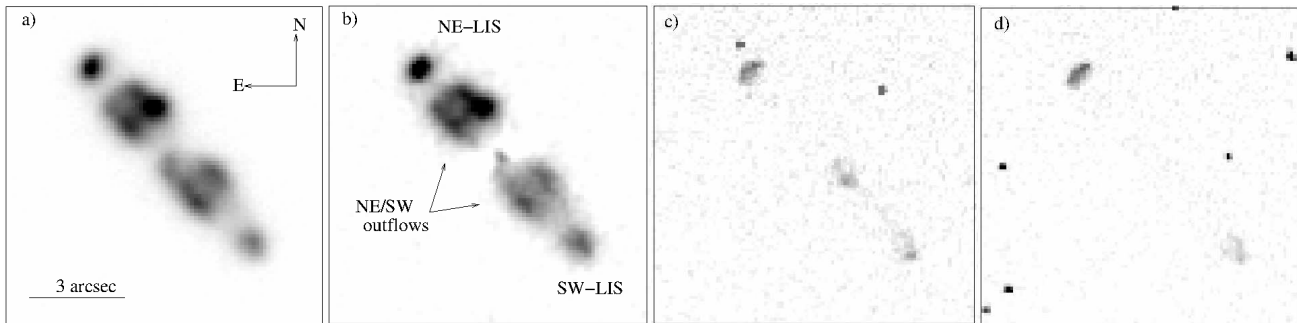


**Figure 1.** Emission line images of K 4-47: (a) NIRI H<sub>2</sub> v=1-0 S(1); (b) NIRI H<sub>2</sub> v=2-1 S(1); (c) *HST* [N II]  $\lambda$ 6584; and (d) *HST* [O I]  $\lambda$ 6300. The size of the boxes is  $20 \times 20$  arcsec<sup>2</sup>. NE-LIS and SW-LIS correspond to Knot1 and Knot2, respectively, in Corradi et al. (2000) and Gonçalves et al. (2004).

lowed us to subtract the continuum contribution from the line emission. Details about the observations are given in Table 1.

The exposure times were estimated using the empirical relation between the fluxes of [O I] 6300 Å and H<sub>2</sub> v=1-0 lines, as reported by Reay et al. (1988). These times (total integration times) and the number of individual frames are summarized in Table 1. GCAL flats frames were also obtained for the correction of thermal emission, dark current and hot pixels, in accordance with the Gemini baseline calibrations. For the correction of sky background as well as bad pixels, the target was dithered across the CCD detector. In order to flux-calibrate the images, we also observed the infrared standard stars FS108 (RA: 03 01 09.8, Dec: +46 58 47.8) and FS 104 (RA: 01 04 59.6, Dec: +41 06 31.3) (Hawarden et al. 2001).

The images were reduced using the tasks within the Gemini IRAF package for NIRI (*Nprepro*, *Nsky*, *Niflat*, *Nireduce* and *Imcoadd*). Before starting the data reduction, the python routines *CLEARIR.py* and *NIRLIN.py* were used in order to correct the vertical stripping and the non-linearity of the detector, which affected the raw data. The reduced H<sub>2</sub> images are presented in Figure 1. The continuum subtracted Br $\gamma$  images of K 4-47 and NGC 7662 are not shown here because either they are too noisy (K 4-47) or the morphology is very similar to the optical *HST* image (NGC 7662). Br $\gamma$  emission in K 4-47 probably originates from the inner core of the nebula, and is very weak in the bipolar outflows and knots. Fig. 2 shows the Br $\gamma$  emission image of K 4-47 (not continuum subtracted), overlaid with the contours of the H<sub>2</sub> v=1-0 emission line.

The  $3\sigma$  detection limits of the H<sub>2</sub> v=1-0 S(1) and Br $\gamma$  line images are  $2.7 \times 10^{-16}$  erg cm<sup>-2</sup> s<sup>-1</sup> arcsec<sup>-2</sup> and  $9 \times 10^{-16}$  erg cm<sup>-2</sup> s<sup>-1</sup> arcsec<sup>-2</sup>, respectively. For the H<sub>2</sub> v=2-1 S(1) line images the  $3\sigma$  are  $1.1 \times 10^{-16}$  erg cm<sup>-2</sup> s<sup>-1</sup> arcsec<sup>-2</sup>, for the K 4-47, and  $2.5 \times 10^{-16}$  erg cm<sup>-2</sup> s<sup>-1</sup> arcsec<sup>-2</sup>, for the NGC 7662, due to the use of different number of frames (see Table 1).

### 3 RESULTS

#### 3.1 The highly collimated PN K 4-47

Optical images of K-4-47 have revealed a jet-like, highly collimated structure with a pair of fast-moving knots (Corradi

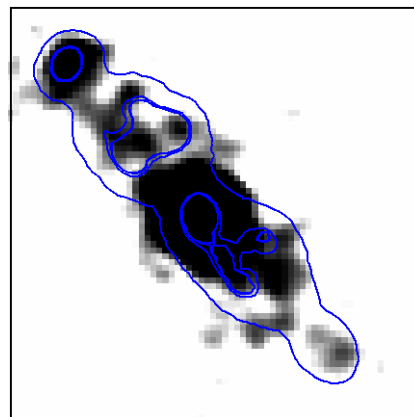


**Figure 2.** Contours of the H<sub>2</sub> v=1-0 S(1) line, overlaid on the Br- $\gamma$  image of K 4-47 (not continuum subtracted). The box size is  $9 \times 9$  arcsec<sup>2</sup>. North is up and east is to the left.

et al. 2000). These knots (where NE-LIS and SW-LIS correspond to Knot1 and Knot2, respectively, in Corradi et al. (2000) and Gonçalves et al. (2004)) exhibit very strong [N II] and [O I] emission lines ([N II] 5200/H $\alpha$ =367 (NE-LIS) and 410 (SW-LIS) and [O I] 6300/H $\alpha$ =427 (NE-LIS) and 305 (SW-LIS), probably implying a strong shock interaction, which is consistent with their high projected expansion velocities of  $\sim 100$  km s<sup>-1</sup> (Corradi et al. 2000). The *HST* [N II]  $\lambda$ 6584 and [O I]  $\lambda$ 6300 images display strong emission in these knots (see Fig. 1, panels c and d, respectively). The distance of the knots from the central star – 3.9 arcsec (NE-LIS) and 3.45 arcsec (SW-LIS) – are slightly different from the values measured by Corradi et al. (2000). However, the distances measured in the optical *HST* images agree better with Corradi et al.’s values.

After analyzing a number of shock models, Gonçalves et al. (2004) came to the conclusion that in order to reproduce the line intensities (or the excitation of the LISs) of this nebula, expansion velocities up to 250-300 km s<sup>-1</sup>, in conjunction with the UV-photons from the central star, are required. Although, the true nature of K 4-47 still remains unknown (is it really a PN, or it could be a symbiotic?), the mechanism responsible for the prominent low-ionization lines is at least partially a result of shock interactions.

From the point of view of molecular chemistry, K 4-47 is a very interesting object, in which many molecules species

**Table 2.** Emission line fluxes for K 4-47, in units of  $10^{-15}$  erg s $^{-1}$  cm $^{-2}$ .  $R(\text{H}_2) = \text{H}_2 \text{ v}=1-0/\text{v}=1-2$  and  $R(\text{Br}\gamma) = \text{H}_2 \text{ v}=1-0/\text{Br}\gamma$ . Numbers in parenthesis correspond to the errors. Fluxes without errors correspond to the  $3\sigma$  upper limits, whereas ratios without errors correspond to lower limits. Radii are in units of arcseconds.

Name	RA	Dec	H <sub>2</sub> v=1-0	H <sub>2</sub> v=2-1	Br $\gamma$	R(H <sub>2</sub> )	R(Br $\gamma$ )	Radius
NE-LIS	04:20:45.5	56:18:16.2	6.82 (0.31)	0.96 (0.05)	0.96	7.12 (0.43)	7.05	0.585
SW-LIS	04:20:44.9	56:18:10.6	4.29 (0.19)	0.64 (0.04)	0.96	6.71 (0.39)	4.47	0.585
NE-outflow	04:20:45.4	56:18:14.8	21.89 (0.45)	2.57 (0.06)	2.47	8.51 (0.23)	8.86	0.936
SW-outflow	04:20:45.1	56:18:12.4	18.38 (0.31)	1.83 (0.05)	2.47	10.05 (0.24)	7.45	0.936

have been found. Huggins et al. (2005) first detected strong CO emission, and few years later Edwards et al. (2014) detected emission in HCO $^+$  and CS. Very recently, HCN emission was also detected in this object (Schmidt and Ziurys 2016). It should be noted, however, that the H<sub>2</sub> densities of K 4-47 calculated by Edwards et al. (2014) and Schmidt and Ziurys (2016) differ by a factor of 10. This discrepancy may be a result of the assumption of Schmidt and Ziurys (2016) that the molecules exist in dense clumps.

We present here the first narrow-band near-IR H<sub>2</sub> images of K 4-47. These images display a remarkable highly collimated bipolar structure, with the emission arising from the walls of the bipolar outflows, resembling a hollow conical structure, and a pair of low-ionization knots apparent at the tips of these outflows (Fig. 1). The detection of H<sub>2</sub> emission in the outflows of K 4-47 proves that the assumption of Schmidt and Ziurys (2016) is not suitable for this object. Furthermore, none of these structures is detected in our Br $\gamma$  images. We thus obtain an upper limits of the Br $\gamma$  line, in order to perform further relevant analysis in Section 4. It should be noted that Lumsden et al. (2001) reported a Br $\gamma$  flux of  $4.29 \times 10^{-15}$  erg s $^{-1}$  cm $^{-2}$  integrated along the slit (2.4 arcsec  $\times$  9.6 arcsec). This emission likely originates mainly from the core of K 4-47. From an inner region of 1.35 arcsec $^2$ , we calculate  $F(\text{Br}\gamma) = (3.3 \pm 0.29) \times 10^{-15}$  erg s $^{-1}$  cm $^{-2}$ .

### 3.2 The elliptical planetary nebula NGC 7662

NGC 7662 is an elliptical PN that possesses more than two dozen of LISs (knots and one jet-like feature at the southern part), mainly embedded in the outer shell. The expansion velocities of these LISs are of the order of 30 km s $^{-1}$ , except for the southern jet-like feature that has  $V_{\text{exp}} = 70$  km s $^{-1}$  (Perinotto et al. 2004). All these structures are easily discerned in the [N II] image (see Guerrero et al. 2004; Gonçalves et al. 2009) or the *HST* [N II]/[O III] line ratio image, as shown in Fig. 3. Spectroscopic data from these structures have also revealed strong [O I]  $\lambda$ 6300 and [N II]  $\lambda$ 6584 emission lines (Perinotto et al. 2004; Gonçalves et al. 2009). Despite the fact that the former lines are important indicators of shock interaction, most of the LISs in NGC 7662 have low expansion velocities, similar to the overall nebular expansion velocity (Perinotto et al. 2004). Thus, we can ask which mechanism, if not shocks, is responsible for the enhancement of the low-ionization emission lines?

From the point of view of the optical emission line ratios, it cannot be deduced whether the LISs of NGC 7662 are shock-excited or photoionized regions. Although the LISs of NGC 7662 are found to be closer to the regime occupied

by fast low-ionization structure (FLIERS) than the regime of rims and shells in the diagnostic diagrams in Raga et al. (2009), they do lie in a very narrow transition zone between the two regimes (see Fig. 6 in Gonçalves et al. 2009). Therefore, both mechanisms (shocks and UV-radiation) should contribute to the overall excitation of these structures.

We present here deep near-IR images of this nebula. The H<sub>2</sub> v=1-0 S(1) line is detected in several optically identified LISs (Fig. 3, right panel), but only four of them (LIS7, LIS8, LIS20 and LIS26) have H<sub>2</sub> v=2-1 S(1) emission, higher than the  $2\sigma$  level. In Table 3 we list the details for each individual LIS in NGC 7662. From the four LISs with both H<sub>2</sub> lines detected, we estimated  $R(\text{H}_2)$  – the H<sub>2</sub> v=1-0/v=1-2 line ratio – to be between 2 and 3.5, whereas for the others we provide lower limits (Table 3).

The very hot and luminous central star of NGC 7662 ( $T_{\text{eff}} = 95\text{kK}$ ,  $\log(L/L_{\odot}) = 3.42$ ; Henry et al. 2015) emits a large number of high-energy UV-photons (high photoionization rate), which, in conjunction with the low expansion velocities of the LISs, suggests that the LISs in this nebula are photoionized predominantly by the radiation field of the central star (Raga et al. 2008; Gonçalves et al. 2009; Aleman et al. 2011; Akras & Gonçalves 2016). Furthermore, all the LISs in this PN are found to be Br $\gamma$ -bright sources ( $R(\text{Br}\gamma) < 1$ ) with a low  $R(\text{H}_2)$  ratio, which seems to be a common characteristic of photoionized regions (Marquez-Lugo et al. 2015) (*See the Sect. 4 for a more complete discussion*).

## 4 DISCUSSION

Motivated by the paradoxical electron density contrast of LISs and their surrounding medium versus that of the formation models, the H<sub>2</sub> and Br $\gamma$  line images of two PNe have been used here for a more detailed study of LISs.

K 4-47 shows a pair of fast-moving knots at the tips of the collimated bipolar outflows. Strong H<sub>2</sub> lines were detected from the knots and the walls of the bipolar outflows. The  $R(\text{H}_2)$  ratio is found to vary from  $\sim 7$  to 10. These values indicate that the excitation of H<sub>2</sub> gas is powered by shocks, which is consistent with the high expansion velocities of the knots (100 km s $^{-1}$ ; Corradi et al. 2000). The strong neutral emission lines found in the knots ([N I] and [O I]) have also been attributed to shock interactions (Gonçalves et al. 2004).

One way to investigate the excitation mechanism of the H<sub>2</sub> gas is by calculating the  $R(\text{H}_2)$  line ratio. In principle, shock-excited regions exhibit  $R(\text{H}_2) > 10$ , whereas photoionized regions can cover a wider range of  $R(\text{H}_2)$  values, from

**Table 3.** Emission line fluxes for the low-ionization structures of NGC 7662, in units of  $10^{-16}$  erg s $^{-1}$  cm $^{-2}$ .  $R(H_2) = H_2 \text{ v=1-0/v=1-2}$  and  $R(Br\gamma) = H_2 \text{ v=1-0}/Br\gamma$ . Numbers in parenthesis are the errors of the fluxes. Flux without errors correspond to the  $3\sigma$  upper limits, whereas the ratios without errors correspond to lower limits. Radii are in units of arcseconds.

Name	RA	Dec	$H_2 \text{ v=1-0}$	$H_2 \text{ v=2-1}$	$Br\gamma$	$R(H_2)$	$R(Br\gamma)$	radius
LIS1	23:25:54.7	42:32:21.5	1.88(0.17)	1.72	6.18	1.09	0.30	0.468
LIS2	23:25:54.5	42:32:21.6	1.96(0.18)	1.72	6.18	1.14	0.31	0.468
LIS3	23:25:54.6	42:32:17.5	1.05(0.11)	0.96	6.62 (0.15)	1.10	0.16 (0.02)	0.351
LIS4	23:25:54.6	42:32:16.2	4.23(0.35)	1.72	13.8 (0.41)	2.46	0.31 (0.03)	0.468
LIS5	23:25:54.4	42:32:14.8	5.14(0.39)	1.72	21.9 (0.33)	2.99	0.23 (0.02)	0.468
LIS6	23:25:54.7	42:32:15.4	1.38(0.13)	0.96	7.68 (0.15)	1.44	0.18 (0.02)	0.351
LIS7	23:25:54.8	42:32:13.8	8.63(0.31)	2.89(0.15)	37.1 (0.69)	2.99(0.19)	0.23 (0.02)	0.702
LIS8	23:25:54.9	42:32:09.7	12.6(0.51)	4.14(0.21)	62.8 (0.79)	3.04(0.20)	0.20 (0.02)	0.702
LIS9	23:25:54.9	42:32:09.1	3.95(0.24)	1.72	24.5 (0.22)	2.30	0.16 (0.02)	0.468
LIS10 <sup>a</sup>	23:25:54.4	42:32:10.9	1.61(0.26)	1.72	4.94 (0.37)	0.94	0.33 (0.05)	0.468
LIS11 <sup>a</sup>	23:25:54.6	42:32:09.6	1.44(0.29)	0.96	3.94 (0.34)	1.51	0.37 (0.06)	0.351
LIS12 <sup>a</sup>	23:25:54.5	42:32:07.6	1.73(0.27)	0.96	3.85 (0.41)	1.80	0.44 (0.05)	0.351
LIS13	23:25:54.7	42:32:06.7	1.81(0.29)	0.96	21.2 (0.31)	1.89	0.09 (0.02)	0.351
LIS14	23:25:54.8	42:32:05.4	1.59(0.13)	0.96	16.3 (0.19)	1.66	0.10 (0.02)	0.351
LIS15	23:25:54.9	42:32:05.5	1.39(0.11)	0.96	13.8 (0.21)	1.45	0.10 (0.02)	0.351
LIS16	23:25:54.9	42:32:01.2	1.69(0.12)	0.96	28.4 (0.39)	1.76	0.06 (0.02)	0.351
LIS17	23:25:54.7	42:32:00.3	1.59(0.12)	0.96	22.9 (0.32)	1.66	0.07 (0.02)	0.351
LIS18	23:25:54.6	42:31:58.7	1.46(0.13)	0.96	16.8 (0.32)	1.52	0.09 (0.02)	0.351
LIS19a	23:25:53.7	42:31:58.2	5.62(0.35)	1.72	94.7 (1.21)	3.27	0.06 (0.02)	0.468
LIS19b	23:25:53.7	42:31:57.3	4.95(0.37)	1.72	80.9 (0.48)	2.88	0.06 (0.03)	0.468
LIS20	23:25:53.7	42:31:52.0	14.3(0.84)	4.41(0.16)	28.4 (0.79)	3.24(0.22)	0.50 (0.04)	0.702
LIS21	23:25:53.6	42:31:50.4	5.38(0.46)	2.68	9.67	2.01	0.55	0.585
LIS22	23:25:53.5	42:31:48.2	0.96(0.09)	0.96	3.47	1.00	0.28	0.351
LIS23	23:25:53.5	42:31:47.3	1.07(0.11)	0.96	3.47	1.12	0.31	0.351
LIS24	23:25:53.2	42:32:02.9	5.72(0.52)	1.72	37.2 (1.24)	3.33	0.16 (0.02)	0.468
LIS25	23:25:52.9	42:32:01.5	2.26(0.21)	0.96	6.51 (0.19)	2.36	0.35 (0.03)	0.351
LIS26	23:25:52.9	42:31:57.6	11.2(0.54)	5.14(0.22)	45.7 (0.98)	2.18(0.15)	0.25 (0.02)	0.702
LIS27	23:25:53.2	42:31:54.8	6.09(0.33)	3.87	25.9 (0.68)	1.58	0.24 (0.02)	0.702
LIS28	23:25:54.2	42:32:18.8	0.72(0.14)	0.96	10.3 (0.31)	0.75	0.07 (0.02)	0.351

<sup>a</sup> For these LISs the residual emission of the rim has been estimated and subtracted.

2 up to 10, depending on the hydrogen gas density and UV radiation intensity. In particular, low density structures exhibit  $R(H_2)$  values close to 3, in contrast to high density structures ( $>10^5$  cm $^{-3}$ ) that can have  $R(H_2)$  values up to 10. This make it hard to deduce whether the emission lines are produced in photoionized or shock-excited regions (see Black & van Dishoeck 1987; Sternberg & Dalgarno 1989; Burton et al. 1990). K 4-47 has  $R(H_2)$  values between  $\sim 7$  (LISs) and 9-10 (bipolar outflows). These  $R(H_2)$  values imply that the excitation mechanism may not be the same, for the two kinds of structures, owing to the substantial difference in their expansion velocities. Our results suggest that K 4-47 is predominantly excited by shocks in agreement with the previous studies (Corradi et al. 2000; Lumsden et al. 2001). However, a contribution of UV-photons from the central star cannot be ruled out (Gonçalves et al. 2004; Akras & Gonçalves 2016). The non-detection of  $Br\gamma$  emission from the bipolar outflows and knots as well as the faint optical emission (Corradi et al. 2000, Gonçalves et al. 2004) imply a very low contribution from the UV-photons to the excitation of K 4-47.

However, the  $R(H_2)$  ratio alone is not enough to discriminate the shock-excited from photoionized regions, as shown by, for example, Marquez-Lugo et al. 2015. These authors demonstrated that shock-excited regions are also brighter in  $H_2$  than in  $Br\gamma$ . In Table 2, we list the  $3\sigma$   $Br\gamma$

detection as well as the lower limit of the  $R(Br\gamma) = H_2 \text{ v=1-0}/Br\gamma$  line ratio. The knots and bipolar outflows of K 4-47 are found to exhibit  $R(Br\gamma) > 5$ , thus providing further evidence of the shock excitation of this PN (see also Lumsden et al. 2001).

The high  $R(H_2)$  values of the bipolar outflows of K 4-47 were unexpected. A comparison of our near-IR image with the optical images from Corradi et al. (2000) reveals that the ionized gas (optical emission) is concentrated in an inner highly collimated structure, which is surrounded by the  $H_2$  bipolar outflows (Fig. 2). These structures of K 4-47 very closely resembles those of M 2-9 (Smith et al. 2005) and CRL 618 (Balick et al. 2013), suggesting a possible connection among these objects.

Recent hydrodynamic models by B. Balick and collaborators (Balick et al. 2013) provide a plausible explanation for the formation of the bipolar outflows in CRL 618. Naively comparing, the same model can adequately explain our findings for K 4-47. The  $H_2$  emission at the walls of the bipolar outflows can be explained by the interactions between a jet or a bullet ejected from the central source with the surrounding AGB material. As the jet/bullet moves through the AGB material, it forms a conical structure that expands laterally outwards. At the same time, the jet/bullet continues moving outwards, with a velocity proportional to the distance from the central star, while dissociating the AGB  $H_2$  gas, which

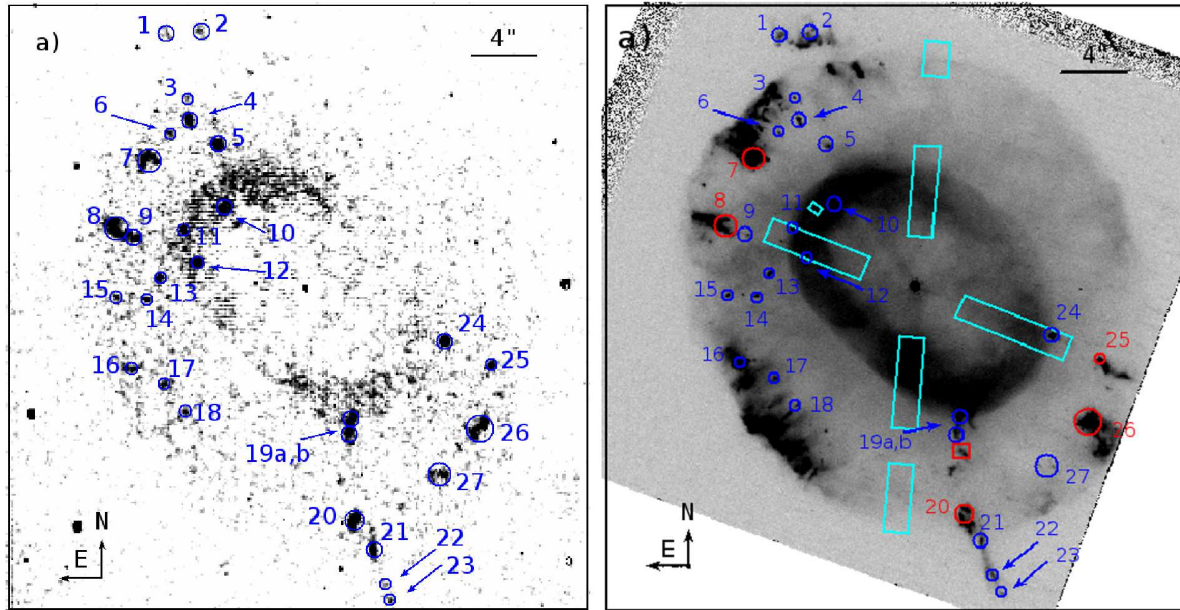


**Figure 3.** Emission line images of NGC 7662: a) NIRI  $H_2$   $v=1-0$   $S(1)$  continuum-subtracted; and b) *HST*  $[N\ II]/[O\ III]$  line ratio image. The circles (in both panels) correspond to the LISs detected in  $H_2$ . The red circles and cyan boxes in panel (b) indicate LISs and nebular regions with available optical spectra (Perinotto et al. 2004, Gonçalves et al. 2009). Both structures have been used in the optical diagnostic diagram (Fig. 5). The red box indicates a LIS with available optical spectrum but not detected in  $H_2$  emission. The box size is  $35 \times 37$  arcsec $^2$ .

then is ionized by the UV-photons emitted from the central star (optical emission). The models also predict strong near-IR  $[Fe\ II]$   $\lambda 1.644\ \mu m$  emission at the outer layers of the knots, owing to the high expansion velocities. Unfortunately, the spectrum obtained by Lumsden et al. (2001) does not cover this line.

In view of the fact that the lateral expansion of the outflows and the velocity of the knots will slow down with time, we predict that the  $H_2$  conical structure observed in K 4-47 will change with time to a more cylindrical shape, similar to the  $H_2$  structure in M 2-9 (Smith et al. 2005). This  $H_2$  emission is, however, attributed to the stellar UV-photons (Kastner et al. 1996) rather than shock interactions. This difference from K 4-47 may be the result of the different evolutionary stage of the nebulae. In particular, K 4-47 has a kinematic age between 400 and 900 yr, depending on the distance (see Corradi et al. 2000), whereas M 2-9 is more evolved with a kinematic age of 2500 yr (e.g. Corradi et al. 2011). This may indicate that PNe like these two are predominantly shock-excited, and that as the central star evolves to a more luminous and hotter phase, the nebula becomes photoionized. By studying objects from different evolutionary stages, Gledhill and Forde (2015) reached the same conclusion. In particular, the  $Br\gamma$  emission increases with time (e.g. IRAS 18062+2410), whereas the  $H_2$  emission is stronger in the post-AGB phase and weaker in the more evolved phase of pre-PNe (e.g. IRAS 20462+3416), or even absent in the most advanced phase of PNe (e.g. IRAS 19336-0400). This implies that the  $R(H_2)$  line ratio decreases with time. Theoretical models for different core masses have shown that the  $R(H_2)$  ratio is strongly dependent on time (evolutionary phase) (see Fig. 18 in Natta and Hollenbach 1998).

Regarding the elliptical PN NGC 7662, the  $H_2$  emission was detected for the first time in LISs, whereas no emission associated with the nebular shells is found. This suggests that molecular  $H_2$  gas in NGC 7662 is probably formed in clumpy structures, as LISs. Recently, van Hoof et al. (2010) investigated three different scenarios for  $H_2$  formation in NGC 6720, through detailed photo-ionization modelling. These authors argued that the most plausible scenario for  $H_2$  formation in NGC 6720 is inside the dense knots formed after the ionization phase, while they ruled out the scenario in which the  $H_2$  gas survives in AGB knots. In contrast to this, it is curious to note that Matsuura et al. (2009) came to the exact opposite conclusion about the  $H_2$  formation in the knots of the Helix nebula. If we compare the survival time of the knots of NGC 6720, 1500-15000 yr (as estimated by van Hoof et al. 2010), and the kinematical age of NGC 7662,  $\sim 1600$  yr ( $1050 \times \frac{D}{800}$ , where  $D=1.2$  kpc; Cahn et al. 1992), both scenarios are feasible for this nebula. Detailed modelling and deep spectroscopic data are necessary in order to obtain an accurate estimate of the survival times and the formation time-scales of the knots, which in turn will lead to a better understanding of how the  $H_2$  condensations or LISs of NGC 7662 were formed.

In contrast to the high-velocity knots in K 4-47, the LISs in NGC 7662 exhibit low expansion velocities of  $30\ km\ s^{-1}$  (Perinotto et al. 2004). Hence, the excitation of these LISs is probably the photoionization by the central star and not by shocks. This hypothesis is in agreement with the very low  $R(H_2)$  ratio of 2 to 3 found in this nebula (see Table 3). As noted above,  $R(H_2)$  alone cannot provide any robust excitation mechanism classification. Shock-excited regions are found to be systematically brighter in  $H_2$  than in  $Br\gamma$  ( $R(Br\gamma) > 1$ ), whereas the photoionized regions are brighter

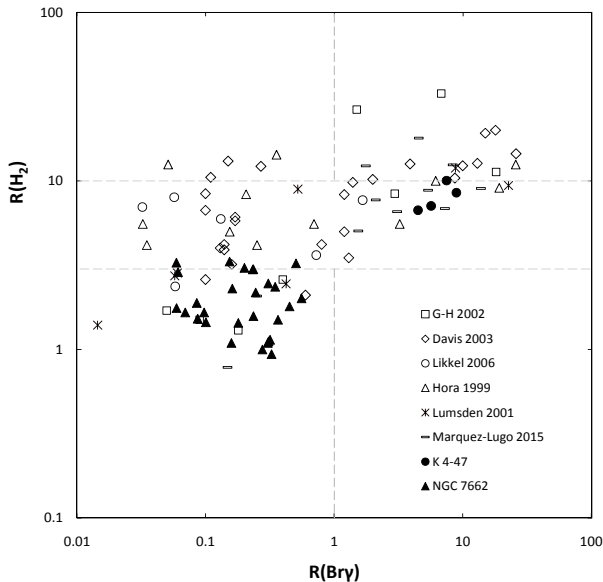


**Figure 4.**  $R(H_2)$  versus  $R(Br\gamma)$  line ratio diagram from Marquez-Lugo et al. (2015) including the values of K 4-47 (filled circles) and NGC 7662 (filled triangles).

in  $Br\gamma$  ( $R(Br\gamma) < 1$ ) (Marquez-Lugo et al. 2015). This trend may reflect the correlation between the  $Br\gamma$  line and the mass of the central star. In particular, massive stars or low-mass stars within the time interval from 1000 to 8000 yrs have  $R(Br\gamma) < 1$  (see Natta & Hollenbach 1998). The low mass ( $0.605M_\odot$ ) central star of NGC 7662 (Guerrero et al. 2004) and its kinematical age of  $\sim 1600$  yr imply a  $R(Br\gamma)$  lower than 1 (see Fig. 18 in Natta & Hollenbach 1998), in agreement with our results in Table 3.

In Fig. 4, we plot the  $R(H_2)$  versus  $R(Br\gamma)$  ratios of all the LISs in this work (K 4-47 and NGC 7662), together with the results from the census by Marquez-Lugo et al. (2015). We find that LISs in NGC 7662 are located in the locus of  $Br\gamma$ -bright source, where the photoionized regions are placed, whereas the bipolar outflows as well as the pair of fast-moving knots in K 4-47 are found in the regime of  $H_2$ -bright sources, where the main excitation mechanism is shocks.

In addition to the  $R(H_2)$  versus  $R(Br\gamma)$  plot, the new optical diagnostic diagram  $[N II]/H\alpha$  versus  $\log(f_{shocks}/f_\star)$  by Akras & Gonçalves (2016) –  $f_{shocks}$  and  $f_\star$  are the ionization photon fluxes owing to the shocks and the central star ionizing continuum – was also used to determine the excitation mechanism of LISs in K 4-47 and NGC 7662. The spectroscopic line ratios of the six LISs in this work (two knots of K 4-47 and four knots of NGC 7662) were gathered from the literature (Perinotto et al. 2004; Gonçalves et al. 2004, 2009).  $D=5.9$  kpc and  $D=1.2$  kpc are adopted for K 4-47 (Goncalves et al. 2004) and NGC 7662 (Cahn et al. 1992; Henry et al. 2015), respectively. We conclude that the knots of K 4-47 are predominantly shock-excited with  $\log(f_{shocks}/f_\star) > 0$ , whereas the LISs in NGC 7662 are found to lie in the transition zone with  $-2 < \log(f_{shocks}/f_\star) < -1$ , where the two mechanisms, shocks and UV-photons, are equally important (Fig. 5). On other hand, regions of the outer shell and rim of NGC 7662 the cyan boxes in Fig. 5) are found to be very close to the regime of photoionized struc-

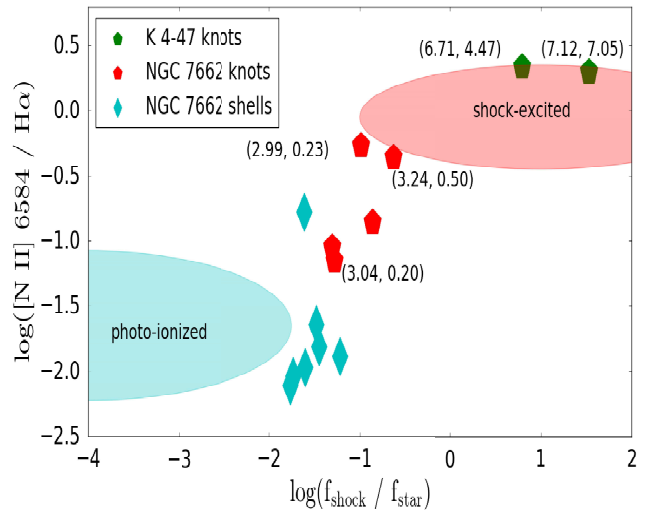


**Figure 5.** The diagnostic diagram for photo-ionized and shock-excited regions by Akras & Gonçalves (2016). The data for K 4-47 and NGC 7662 were obtained from Gonçalves et al. (2009) and Perinotto et al. (2004), respectively. The numbers in parenthesis indicate the value of  $R(H_2)$  and  $R(Br\gamma)$ . (A color version of this figure is available in the online journal.)

tures. This result strengthens our previous analysis that shocks have altered the ionization structure of LISs.

## 5 CONCLUSION

The deepest ever high-angular-resolution, near-IR narrow-band  $H_2$   $v=1-0$  S(1),  $H_2$   $v=1-2$  S(1) and  $Br\gamma$  images of two Galactic PNe with LISs (K 4-47 and NGC 7662) have been presented in this work.  $H_2$  was detected in both high-velocity knots (K 4-47) and low-velocity knots (NGC 7662) as well as at the walls of the bipolar outflows of K 4-47. Therefore, we confirm that LISs are indeed partially made of  $H_2$  gas, which, in conjunction with their strong optical low-ionization emission lines, strongly suggest that LISs are probably mini-PDRs embedded in the nebulae. The  $H_2$  emission was found to be excited either by shocks (K 4-47) or by high-energy UV-photons (NGC 7662). Moreover, the bright  $H_2$  emission lines that emanated from the walls of the bipolar outflows of K 4-47 are consistent with the prediction of hydrodynamic models. In summary, these predictions are that a jet/bullet ejected from the central star interacts with the AGB remnant matter producing a conical structure that expands laterally. As the jet/bullet continues moving outwards, it dissociates the AGB materials, which later it is ionized by the UV radiation field of the central star. Moreover, we concluded that K 4-47 and M 2-9 may be akin young PNe in different evolutionary stage.

Additional deep (8 m class telescopes and similar), high-angular-resolution observations of PNe with LISs are required in order to cover a wider range of parameters ( $T_{eff}$ ,  $L$ , expansion velocities,  $n_e$ ) and provide a definitive understating of the excitation and formation mechanisms of the low-ionization structures of PNe.

**ACKNOWLEDGMENTS**

We are extremely grateful to the anonymous referee for his constructive and helpful report. S.A. is supported by the CAPES Brazilian post-doctoral fellowship “Young Talents Attraction” - Science Without Borders, A035/2013. GRL acknowledges support from CONACyT and PROMEP (Mexico). The observations we report here were obtained at the Gemini Observatory (processed using the Gemini IRAF package and Gemini-python), which is operated by the Association of Universities for Research in Astronomy, Inc., under a cooperative agreement with the NSF on behalf of the Gemini partnership: the National Science Foundation (United States), the National Research Council (Canada), CONICYT (Chile), the Australian Research Council (Australia), Ministério da Ciência, Tecnologia e Inovação (Brazil) and Ministerio de Ciencia, Tecnología e Innovación Productiva (Argentina). This research is also based on observations made with the NASA/ESA Hubble Space Telescope, and obtained from the Hubble Legacy Archive, which is a collaboration between the Space Telescope Science Institute (STScI/NASA), the Space Telescope European Coordinating Facility (ST-ECF/ESA) and the Canadian Astronomy Data Centre (CADC/NRC/CSA).

**REFERENCES**

- Akras S., Gonçalves D. R., 2016, *MNRAS*, 455, 930A  
 Akras, S., Clyne, N., Boumis, P., Monteiro, H., Gonçalves, D. R., Redman, M. P., Williams, S., 2016, *MNRAS*, 457, 3409  
 Aleman I., Gruenwald R., 2004, *ApJ*, 607, 865  
 Aleman I., Zijlstra A. A., Matsuura M., Gruenwald R., Kimura R. K., 2011, *MNRAS*, 416, 790  
 Aleman I., Gruenwald R., 2011, *A&A*, 528, 74.  
 Arias L., Rosado M., Salas L., Cruz-González I., 2001, *AJ*, 122, 3293  
 Balick B., 1987, *AJ*, 94, 671  
 Balick B., Rugers M., Terzian Y., Chengalur J. N. 1993, *ApJ*, 411, 778  
 Balick B., Perinotto M., Maccioni A., Terzian Y., Hajian A., 1994, *ApJ*, 424, 800  
 Balick B., Alexander J., Hajian A., Terzian Y., Perinotto M., Patriarchi P., 1998, *AJ*, 116, 360.  
 Balick B., Huarte-Espinosa M., Frank A., Gomez T., Alcolea J., Corradi R. L. M., Vinković D., 2013, *ApJ*, 772, 20B  
 Bohigas J., 2001, *RevMexAA*, 37, 237.  
 Burton M. G., Hollenbach D. J., Tielens A. G. G. M., 1990, *ApJ*, 365, 620  
 Cahn J. H., Kaler J. B., Stanghellini L., 1992, *A&AS*, 94, 399  
 Corradi R. L. M., Manso R., Mampaso A., Schwarz H. E., 1996, *A&A*, 313, 913.  
 Corradi R. L. M., Gonçalves D. R., Villaver E., Mampaso A., Perinotto M., Schwarz H. E., Zanin C., 2000, *ApJ*, 535, 823  
 Corradi R. L. M., Balick B., Santander-García, M., 2011, *A&A*, 529, 43  
 Davis C. J., Smith M. D., Stern L., Kerr T. H., Chiar J. E., 2003, *MNRAS*, 344, 262  
 Dopita, M. A. 1997, *ApJ*, 485, 41  
 Edwards J. L., Cox E. G., Ziurys L. M., 2014, *ApJ*, 791, 79  
 Fang, X., Guerrero, M. A., Miranda L. F., Riera A., Velázquez P. F., Raga A. C., 2015, *MNRAS*, 452, 2445  
 García-Hernández D. A., Manchado A., García-Lario P., Domínguez-Tagle C., Conway G. M., Prada F., 2002, *A&A*, 387, 955  
 García-Segura G., López J. A., Franco J., 2005, *ApJ*, 618, 919  
 Gledhill T. M., Forde K. P., 2015, *MNRAS*, 447, 1080  
 Gonçalves D. R., Corradi R. L. M., Mampaso A., 2001, *ApJ*, 547, 302  
 Gonçalves D. R., Corradi R. L. M., Mampaso A., Perinotto M., 2003, *ApJ*, 597, 975  
 Gonçalves D. R., Mampaso A., Corradi R. L. M., Perinotto M., Riera A., López-Martín L., 2004, *MNRAS*, 355, 37  
 Gonçalves D. R., Mampaso A., Corradi R. L. M., Quireza C., 2009, *MNRAS*, 398, 2166.  
 Guerrero M. A., Villaver E., Manchado A., García-Lario P., Prada F., 2000, *ApJS*, 127, 125  
 Guerrero M. A., Jaxon E. G., Chu Y.-H., 2004, *AJ*, 128, 1705G  
 Hawarden T. G., Leggett S. K., Letawsky M. B., Ballantyne D. R., Casali M. M., 2001, *MNRAS*, 325, 563  
 Henry R. B. C., et al., 2015, *ApJ*, 813, 121  
 Hora J. L., Latter W. B., Deutsch L. K., 1999, *ApJS*, 124, 195  
 Hrivnak J B., Smith N., Su Y. L K., Sahai R., 2008, *AJ*, 688, 327  
 Huggins P. J., Forveille T., Bachiller R., Cox P., Ageorges N., Walsh J. R., 2002, *ApJ*, 573, 55  
 Huggins P. J., Bachiller R., Planesas P., Forveille T., Cox P., 2005, *ApJS*, 160, 272  
 Kastner J. H., Gatley I., Merrill K. M., Probst R., Weintraub D., 1994, *ApJ*, 421, 600  
 Kastner J. H., Weintraub D. A., Gatley I., Merrill K. M., Probst R. G., 1996, *ApJ*, 462, 777.  
 Latter W. B., Kelly D. M., Hora J. L., Deutsch L. K., 1995, *ApJS*, 100, 159  
 Likkell L., Dinerstein H. L., Lester D. F., Kindt A., Bartig K., 2006, *AJ*, 131, 1515  
 Lumsden S. L., Puxley P. J., Hoare M. G., 2001, *MNRAS*, 328, 419  
 Manchado A., Stanghellini L., Villaver E., García-Segura G., Shaw R. A., García-Hernández D. A., 2015, *ApJ*, 808, 115  
 Marquez-Lugo R. A., Ramos-Larios G., Guerrero M. A., Vázquez R., 2013, *MNRAS*, 429, 973  
 Marquez-Lugo R. A., Guerrero M. A., Ramos-Larios G., Miranda L. F., 2015, *MNRAS*, 453, 1888  
 Matsuura M., et al., 2009, *ApJ*, 700, 1067  
 Natta A., Hollenbach D., 1998, *A&A*, 337, 517  
 Perinotto M., Patriarchi P., Balick B. and Corradi R. L. M., 2004, *A&A*, 422, 963P  
 Phillips J. P., 2006, *MNRAS*, 368, 819  
 Phillips J. P., Ramos-Larios G., Guerrero M.A., 2011, *MNRAS*, 415, 513  
 Raga A. C., Riera A., Mellema G., Esquivel A., Velázquez P. F., 2008, *A&A*, 489, 1141R  
 Ramos-Larios G., Guerrero M. A., Vázquez R., Phillips J. P., 2012, *MNRAS*, 420, 1977.

- Ramos-Larios G., Guerrero M. A., Vázquez R., 2013, MNRAS, 429, 973.
- Reay, N. K., Walton N. A., Atherton, P. D, 1988, MNRAS, 232, 615
- Sahai R., et al., 1998, ApJ, 492, 163
- Schmidt D. R., Ziurys L. M., 2016, ApJ, 817, 175
- Smith N., Balick B., Gehrz R. D., 2005, AJ, 130, 853
- Soker N., Livio M., 1994, ApJ, 421, 219
- Steffen W., López J. A., Lim A., 2001, ApJ, 556, 823
- Sternberg A., & Dalgarno A., 1989, ApJ, 338, 197